Impact of superficial surface texture anisotropy in helical slide and plateau honing on ring-pack performance

Ibrahim Demirci[1], S Mezghani[1], M Yousfi[1,2] and M El Mansori[3]

Abstract

The improvement of environment efficiency of automotive internal combustion engine becomes a fundamental objective. The cylinder engine surface texture considerably influences the functional performances of the ring-pack tribo-system. These surfaces are obtained by honing process that was pioneered in the last decade. Several innovative honing techniques were developed resulting in new surface textures with different cross-hatch angle obtained after several stages: the rough and finish honing and final stage. The aim of this study is to investigate the effect of variable cross-hatch angle generated at a final stage. These measured obtained surfaces are measured by a 3D white light interferometer and used as input data of the numerical model to estimate the friction. The results show the importance of this 'residual' angle.

Introduction

Improving energy efficiency in the automotive industry has become essential in view of the stringent legislation on reducing carbon emission. Despite efforts on weight reduction of vehicles and integration of car electronics, energy efficiency of cars (and thus reduction of carbon emissions) will be improved by reducing the friction generated between the mechanical parts in contact. Especially, cylinder engine surface texture considerably influences the functional performances (running-in, friction, oil consumption, wear, etc) of the ring-pack tribo-system.[1–5] Indeed, the surface features of a cylinder liner engine are the fingerprint of the successive processes the surface has undergone, and they influence the functional performance of the combustible engine.[5–11]

Generally, the process used for cylinders surfaces is honing after drilling or turning operation. This guaranties the reproducibility with efficient productivity in mass production of cylinder liners.[12] In this process, abrasive stones are loaded against the bore and simultaneously rotated and oscillated. The obtained surface textures should ensure quick running-in, minimum friction during sliding, low oil consumption and good motor engine-operating parameters in terms of effective power and unitary fuel consumption. The industrial honing uses coarse abrasive stones at first and then progressively, finer grades, resulting in a very structured surface of liner.[13] Several efforts have been made to improve the honing process for cylinder liner finishing. Innovative honing techniques, such as helical slide honing, glade honing and brush honing,[8,14–17] were developed resulting in new surface textures. These textures are principally composed by two sets of straight, approximately parallel grooves placed stochastically and appearing at different angles to the cylinder axis.[18,19] The angle between the honing grooves perpendicular to the cylinder axis is named as the cross-hatch angle. This angle is obtained after several stages: first of all, the rough honing – in the second stage named finish honing basic surfaces – is generated with a given cross-hatch angle and then the final stage that confers different honing angle in our study.

The honed surface texture can be divided into two principal components: plateaus and valleys with depth greater than the surface roughness.[19] These geometric properties of cylinder bores affect considerably the

[1]Arts et Métiers ParisTech, MSMP Rue saint Dominique, Chalons-en-Champagne, France
[2]Renault s.a.s. Direction de l'ingénierie Mécanique C67 rue des bons raisons, 92500 Rueil Malmaison, France
[3]Arts et Métiers ParisTech, MSMP Cours des Arts et Métiers, Aix-en-Provence, France

Corresponding author:
Ibrahim Demirci, Arts et Métiers ParisTech, MSMP Rue saint Dominique, 51006 Chalons-en-Champagne, France.
Email: ibrahim.demirci@ensam.eu

functional performances of the ring pack contact, especially, superficial roughness,[20,21] the valley and surface patterns depth and density[22] and the cross-hatch angle.[3,4,22–24] For example, with plateau honing (PH), cross-hatch angle is about 50° whereas with helical slide-honing process (HSH) is about 130°. These two angles correspond to the optimal ranges of cross-hatch angle in hydrodynamic lubrication condition as demonstrated by Spencer et al.[5] and Mezghani et al.[22] However, with helical slide-honed liners (130° honing angle), friction is much less sensitive to superficial plateau roughness than with the plateau-honed liners (50°).[6]

The aim of this study is to investigate the effect of cross-hatch angle generated at a final stage for two kinds of honing processes: the PH and HSH to determine how the variation of cross-angle at final stage affects the predicted fiction. Thus, cross-hatch angle at the final stage varies in the range of 30°–130° whereas angle at finish honing stage is kept constant: 50° for PH and 130° for HSH.

Measurement procedure

In this work, the honed surfaces were obtained by an instrumented vertical honing machine with an expansible tool (NAGEL, no. 28-8470) (Figure 1). Typically, cast iron crankcase of diesel engines is used. The cylinders are produced by a succession of three honing stages (rough, finish and PH).[25–27] Table 1 shows the most important working variables applied for these tests.

The first stage often named as rough honing establishes the cylindricity of the bore with % = 76.005 ± 0.005 cylinder-liner diameter. The second stage called; 'finish honing' creates the basic surface texture of the hole with a characteristic cross-hatch lay pattern defines as the honing angle. It depends on the axial speed to speed of rotation with respect to the following formula

$$\tan\left(\frac{\alpha}{2}\right) = \frac{V_a}{V_r}$$

where V_a is the axial speed and V_r is the rotation speed. At this stage, two axial and two rotational speeds were considered while the other working variable was kept constant (see Table 1). The use of the following pairs of speed 18 (m min^{-1}) – 160 r/min and 29 (m min^{-1}) – 58 r/min allows generating two levels of cross-hatch angle, respectively, 50° and 130°. These angles will be called α in the rest of the document. The maximum value of 130° is due to a limitation of the honing machine. For the final finishing stage known as 'PH', several axial and rotational speed combinations were used. These speed parameters allow to generate various honing angle, named α_f in the rest of document, ranging from 30° to 130°. For each speed combination, surfaces were measured in three

locations by a three-dimensional white light interferometer, WYKO 3300 NT(WLI). The surface was sampled at 640×480 points with the same step scale of $1.94\,\mu m$ in the x and y directions. Stitching method is used to have an approximate image with the section of $1 \times 2\,mm^2$. Each measure was repeated three times in three different locations in the mid-stroke region of the cylinder liner. This 3D surfaces texture (see Figure 2) of honed surfaces after the plateau-honing stage of the cylinder bore specimen was used as input data in the numerical model to predict friction coefficient.

Mixed numerical model formulation

The real topography measured with the above method is used as input in the developed numerical model to estimate the friction generated. In this model, the ring is approximated by a cylinder and the liner by a plane. Although popular stochastic methods to consider surface roughness developed by Patir and Cheng[28] have significant notoriety, a three-dimensional deterministic model for rough surface is used in our work. This deterministic method allows a more realistic description of the phenomena studied. Moreover, with this method, it is not necessary to determine the pressure and shear flow factors. Thus, this model is a three-dimensional deterministic model for rough surface, and it is based on Hu and Zhu's[29] unified model originally developed for points contact.

Mixed lubrication equations

A generalized Reynolds' equation developed by Yan and Wen[30] has been used to estimate the pressure distribution, film thickness and the friction coefficient. This equation is developed for solving non-Newtonian thermal elastohydrodynamic lubrication problems. It has the advantage of not being restricted to a particular non-Newtonian law. The well-known mass-conserving mathematical model proposed by Elrod and Adams[31] with mass-conserving algorithm developed by Ausas et al.[32] is added to the generalized Reynolds' equation. For transient problems, this takes the following form

$$\frac{\partial}{\partial x}\left[\left(\frac{\rho}{\eta}\right)_e h^3 \frac{\partial p}{\partial x}\right] + \frac{\partial}{\partial y}\left[\left(\frac{\rho}{\eta}\right)_e h^3 \frac{\partial p}{\partial y}\right] = 12\frac{\partial}{\partial x}(\theta\rho^*\bar{u}h) + 12\frac{\partial}{\partial t}(\theta\rho_e h) \tag{1}$$

where

$$\left(\frac{\rho}{\eta}\right)_e = 12\left[\frac{\eta_e\rho'}{\eta'_e} - \rho''\right] \tag{2}$$

$$\rho^* = \frac{\rho'\eta * e'(u_2 - u_1) + \rho_e u_1}{\bar{u}} \tag{3}$$
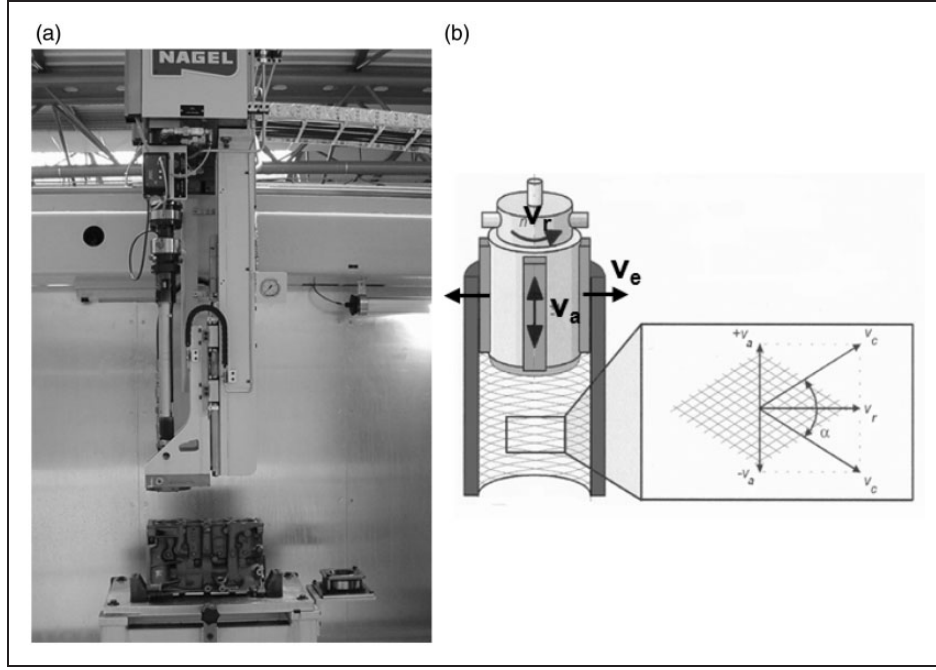
Figure 1. (a) Vertical honing machine with expansible tool; (b) schematic illustration of the honing head in continuous balanced movement.

Table 1. Experimental parameters used in cutting tests.

Honing parameters	Finish rough	Plateau honing
Axial speed (m min^{-1})	18, 29	11, 18, 27, 29
Rotation speed (rate/min)	58, 160	58, 85, 135, 170
Expansion type	Mechanical	Hydraulic
Expansion speed (μm s^{-1})	4	
Contact pressure	6	5,5
Number of stones	4	4
Abrasive grit type	Silicon carbide	Silicon carbide
Cross-hatch angle	50°, 130°	30°, 50°, 80°, 110°, 130°

$$\rho_e = \frac{1}{h} \int_0^h \rho \, \mathrm{d}z \tag{4}$$

$$\rho' = \frac{1}{h^2} \int_0^h \rho \int_0^z \frac{\mathrm{d}z'}{\eta} \mathrm{d}z \tag{5}$$

$$\rho'' = \frac{1}{h^3} \int_0^h \rho \int_0^z \frac{z'\mathrm{d}z'}{\eta} \mathrm{d}z \tag{6}$$

$$\frac{1}{\eta} = \frac{1}{h} \int_0^h \frac{\mathrm{d}z}{\eta} \tag{7}$$

$$\frac{1}{\eta'} = \frac{1}{h^2} \int_0^h \frac{z\mathrm{d}z}{\eta} \tag{8}$$

The boundary conditions of equation (1) are $p \geqslant 0$, $\theta = 1$ on the active region and $p = 0$, $\theta < 1$ at the cavitated region, $p = 0$ on inlet and outlet boundary and with periodicity imposed in y directions. The rheological behaviour of the lubricant used in the present study is the Carreau model, which takes into account the second Newtonian plateau that can occur at very high shear rates. A modified version of this law by Bair[33] is considered

$$\eta = \mu_2 \frac{\mu_1 - \mu_2}{\left[1 + \left(\frac{\tau_c}{G_c}\right)^{\beta_c}\right]^{\frac{\frac{1}{n_c}-1}{\beta_c}}} \tag{9}$$

where G_c is the liquid critical shear stress, β_c and n_c are two constant parameters and μ_1 and μ_2 are the low and high-shear limiting viscosities, respectively, which depend on the pressure and temperature. In this work, Tait equation of state (equation (10)) and Doolittle model (equation (11)) are used for density
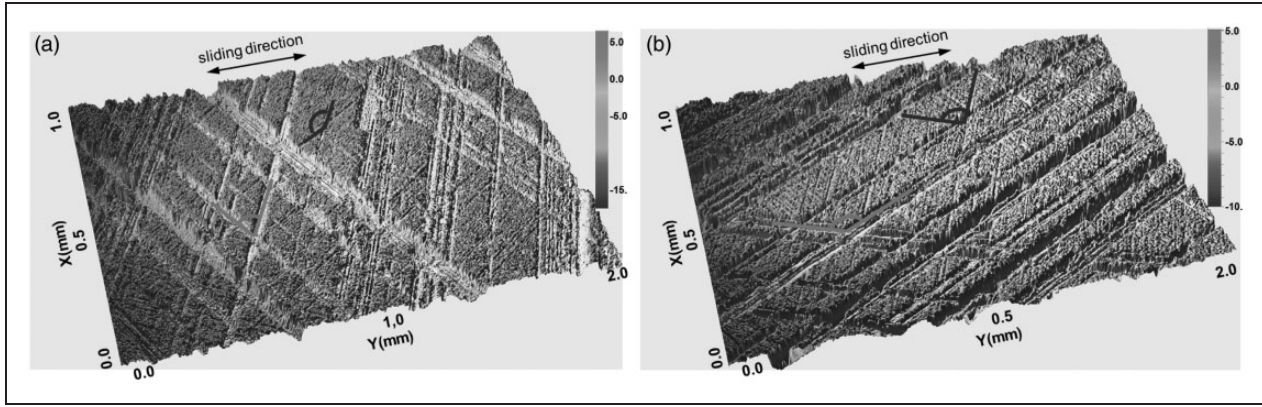
Figure 2. 3D topographies of finish honed surfaces presenting multi-angle surfaces (a) 50°–110°, (b) 130° − 50° (red lines correspond to α, blue to α_f).

and viscosity variations, respectively. The Tait equation of state is written for the volume V relative to the volume at ambient pressure V_0

$$\rho(p, T) = \rho_R \left(\frac{1}{V_0/V_R} \times \frac{1}{V/V_0} \right) \tag{10}$$

where

$$\frac{V_0}{V_R} = 1 + a_v (T - T_R) \tag{11}$$

$$\frac{V}{V_R} = 1 - \frac{1}{1 + K_0'} ln\left[1 + \frac{p}{K_0}(1 + K_0') \right] \tag{12}$$

$$K_0 = K_{0R} \exp(-\beta_K T) \tag{13}$$

$$K_0' = K_{0R}' \exp(\beta_{K'} T) \tag{14}$$

with a_v the volume–temperature variation constant, T_R the reference temperature, K_0 the initial bulk modulus, K_0' the initial pressure rate of change of bulk modulus, β_K the bulk modulus-temperature coefficient and $\beta_{K'}$ the initial pressure rate of change of bulk modulus-temperature coefficient. The physical viscosity–pressure–temperature Doolittle model is given by the following relationship

$$\mu(p, T) = \mu_R \exp\left[BR_0 \left(\frac{\frac{V_\infty}{V_{\infty R}}}{\frac{V}{V_R} - R_0 \frac{V_\infty}{V_{\infty R}}} - \frac{1}{1 - R_0} \right) \right] \tag{15}$$

where V/V_R is described above and

$$\frac{V_\infty}{V_{\infty R}} = 1 + \epsilon_c (T - T_R) \tag{16}$$

B and R_0 are constants characterizing a given lubricant and ϵ_c is the relative-occupied volume-temperature coefficient. The variables used in the above equations are derived from Habchi.[34] The film thickness equation, which takes into account the deformation of elastic bodies over the computational domain, is given by

$$h(x, y, t) = h_0 + \frac{x^2}{2R_x} + \frac{2}{\pi E_r} \int_{-\infty}^{+\infty}$$
$$\frac{p(x', y', t)dx'dy'}{\sqrt{(x - x')^2 + (y - y')^2}} - zh(x, y, t) \tag{17}$$

where E_r is the reduced elastic modulus and zh is the height surface topography of each position (x,y).

Numerical procedure. The above-described equations were solved by the finite difference method. A second-order accuracy was used with respect to both space and time.[35] The discretized equation was solved by the Jacobi line relaxation.[36] The full-scale mixed EHL approach developed by Hu and Zhu[29] was used in the present study. The surface deformation is calculated with the discrete convolution and FFT (DC-FFT) algorithm presented by Liu et al.[37] and advanced forward by Chen et al.[38] At every iteration, the integral terms in the generalized Reynolds equation were calculated using the solution obtained at the previous stage. A classical Newton–Raphson procedure was used to determine the shear stress and the generalized Carreau model viscosity. The solution domain is chosen as 3.5*a from the contact centreline of $x = 0$ and the outlet distance to be 1.5*a (a is the Hertzian contact radius) and $y = 10$ mm. The computational grid covering the domain consisted of equally spaced 513×513 or 1025×1025 nodes. For transient state, NU2 scheme as described in Chapkov[39] is used and dt = dx. Using rough surfaces in EHL, simulation could yield localized asperity contact pressure peaks usually higher than the average EHL pressure. This results in high subsurface stress that exceeds the material yielding limit.[40] To limit the contact pressure, the elastic-perfectly plastic behaviour of a material was approximately simulated by using a cut-off value equal to the hardness of the material. The
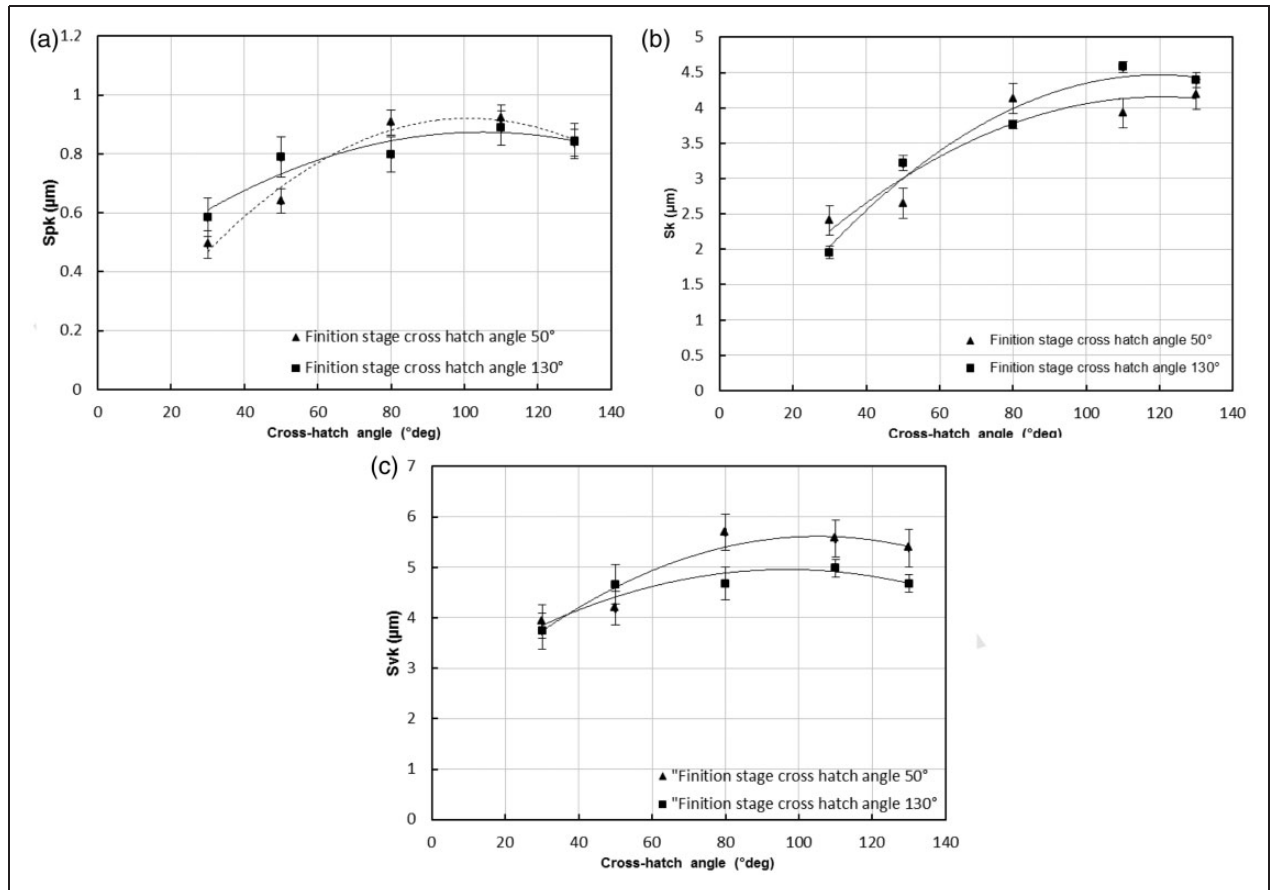
Figure 3. Evolution of (a) S_{pk}, (b) S_k and (c) S_{vk} surface roughness parameter as a function of cross hatch-angle at plateau-honing stage.

validation of the present model was found in Demirci et al.[41]

Results and discussion

In this study, the cylinder liner has a Young modulus and Poisson ratio of 140 GPa and 0.3, respectively. The ring is assumed to have parabolic shape, and ring width is 2.5 mm with Young modulus and Poisson ratio of 220 GPa and 0.3, respectively. Isothermal condition is used in our model (temperature is 303 K). Surface roughness has been evaluated using the normalized 3D functional roughness parameters based on the ISO 25178 standard. These parameters are based on the analysis of a bearing curve, which is simply a plot of the cumulative probability distribution of surface roughness height. These are

S_k depth of roughness core profile;

S_{pk} reduced peak height, average height of the protruding peaks above the roughness core profile;

S_{vk} reduced valley depths, average depth of the profile valleys projecting through the roughness core profile.

Figure 3 displays the evolution of these roughness parameters as a function of cross-hatch angle value.

For small angle, S_{pk} is low for 50° finish stage angle and increases to reach the stable value whereas for 130° finish stage angle, the stable value is reached quickly. However, the S_{pk} values are close for both α_f. As we can see, superficial roughness of honed surfaces is similar to whatever the value of the finish stage angle. S_{vk} parameter slightly increases with the angle for both finish stage angle and there are close. Finally, the generated surfaces during the process are very similar in roughness for both α_f.

The numerical model presented in 'Experimental procedure' was used to predict friction in the ring-liner-piston contact and to analyse the effect of α_f on friction. In this model, measured surfaces were used as input data for numerical model, and we choose 100 N as normal force and 400 r/min for velocity to sweep the lubrication regime, from mixed to hydrodynamic and to stay in a range of the ring-cylinder linear tribometre developed in our laboratory. Generated surfaces will be tested in this experimental apparatus. During the simulation, the velocity was calculated as a function of spindle angle. Running-in and surface change are not taken into account. Figure 4 displays the evolution of mean friction coefficient and the evolution of metal to metal contact as a function of α_f generated at plateau stage. For 50° finish stage-honing angle α_f, the friction coefficient
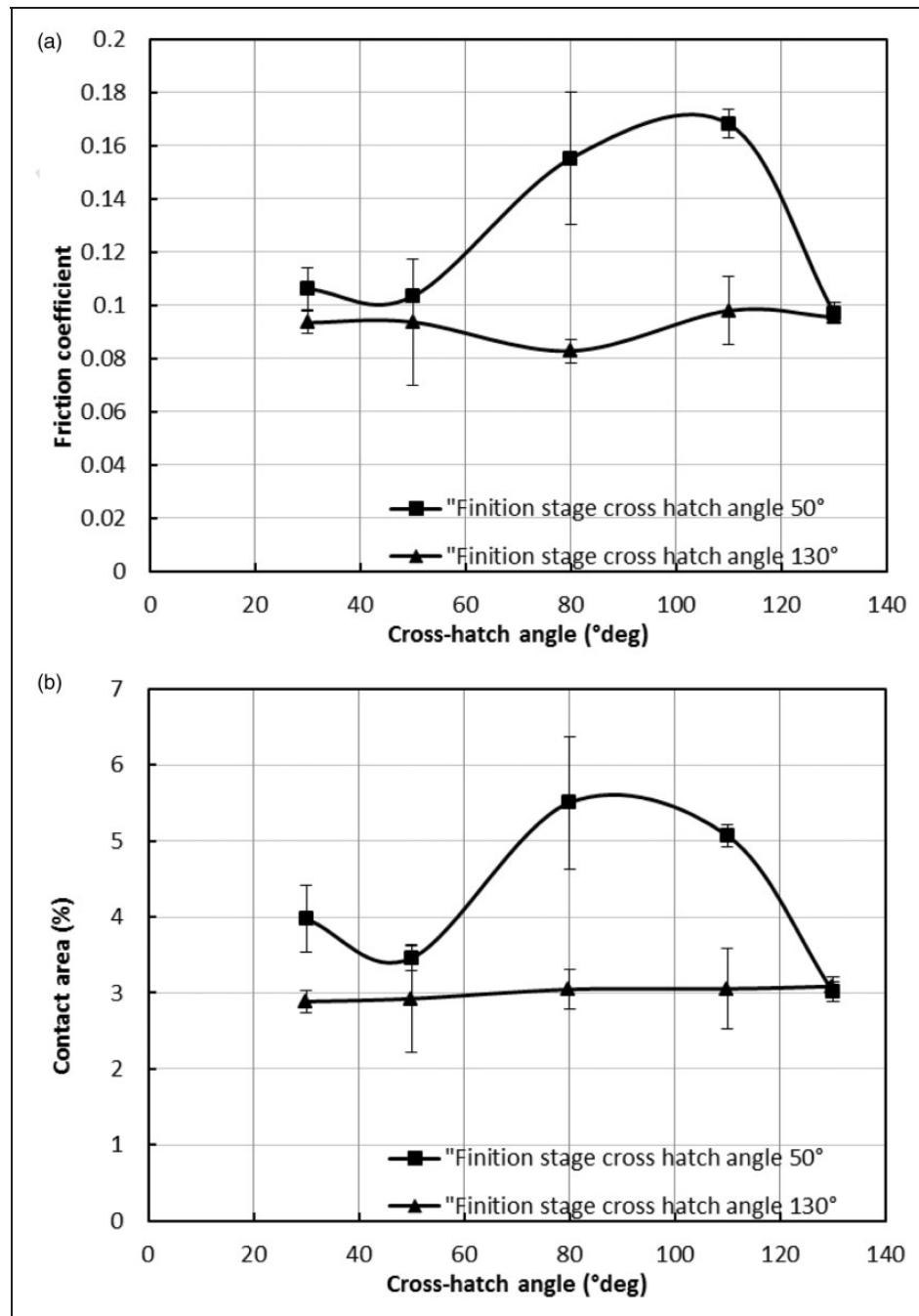
Figure 4. Evolution of (a) friction coefficient and (b) contact area ratio as a function of cross-hatch angle at plateau-honing stage.

increases until a high value and then decreases for a lowest value at $\alpha_f = 130°$. Whereas for the second cross-hatch angle ($\alpha = 130°$), the friction is relatively constant regardless of the value of the honing angle. The variability of friction coefficient due to the variation of α_f for 50° and 130° finish honing angle is, respectively, 26% and 6%. The metal-to-metal contact has the same behaviour as coefficient friction. For 50°, this parameter increases to reach maximum value and then decreases. There is a change of lubrication regime with final stage angle α_f from the mixed regime to the hydrodynamic regime. However, for 130°, the dry contact area is relatively constant, and the lubrication regime is close to a hydrodynamic regime. The

change of α_f does not modify the lubrication regime. The variation of roughness parameters is not constant but random. The size of this type of streak should a priori not affect the surface functionality, but the surface anisotropy of superficial plateau cross hatch-angle for 50° case plays an important role in the friction as already mentioned in Mezghani et al.[6,22]

The frictional performance of helical slide-honed cylinder is less sensitive to α_f (Figure 4). Plateau-honed surface friction is very sensitive to final honing stage as already mentioned by Mezghani et al.[6] Therefore, the final honing stage in PH process has a decisive influence in generating different plateau cross-hatch angle compared to HSH (130°). Especially,

$\alpha_f = 130°$ in final stage in PH process (50° finish honing angle) give the better frictional performance. The process can be easily modified to generate angles of 130° at the plateau stage for improving the frictional performance of the textured surface. In contrary, surface textures with 130° cross-hatch angles are very less sensitive to α_f. Whatever the final stage honing cross-hatch angle α_f, friction is almost identical. Therefore, as for superficial roughness mentioned in Mezghani et al.,[6] the third operation of HSH can be cancelled in the production process. Indeed, $\alpha = 130°$ angle is less sensitive to the anisotropy generated in the final stage and the variability of the angle of grinding. Finally, if an angle of 130° is generated on the surface during process (during finish honing or final stage), frictional performance is less sensitive to residual streaks created in the preceding stages and present on the surface.

Conclusions

The effect of cross-hatch angle generated at final stage honing for two kinds of honing processes was investigated. Two honing angles, 50° honing angle (PH process) and 130° honing angle (HSH), obtained at the second stage, named finishing stage, were considered. Then, several cross-hatch honing angles ranging from 30° to 130° were generated at the third and final stage of process. The obtained surfaces were measured to obtain real 3D surface, which is used as an input data. Then, the friction performance of these surfaces was predicted by the developed numerical model in mixed lubrication regime. The results show that

1. Helical slide-honing angle surface (130°) has the best frictional performance and is independent of third-stage angle.
2. Surface textures with 130° cross-hatch angles at finishing stage are very less sensitive to final honing stage kinematic.
3. For 50° honing angle, friction coefficient is sensitive to the final stage cross-hatch angle.
4. Frictional performance is less sensitive to residual streaks created during the honing process and present on the surface if an angle of 130° is generated during the finish honing of final stage.

Declaration of conflicting interests
The author(s) declared no potential conflicts of interest with respect to the research, authorship, and/or publication of this article.

References

1. Mezghani S, Demirci I, El Mansori M, et al. Energy efficiency optimization of engine by frictional reduction of functional surfaces of cylinder ring-pack system. *Tribol Int* 2013; 59: 240–247.
2. Pawlus P. Effects of honed cylinder surface topography on the wear of piston piston ring-cylinder assemblies under artificially increased dustiness conditions. *Tribol Int* 1993; 26: 49–55.
3. Shinkarenko A, Kligerman Y and Etsion I. The effect of surface texturing in soft elasto-hydrodynamic lubrication. *Tribol Int* 2009; 42: 284–292.
4. Jocsak J, Wong VW and Tian T. The effects of surface finish on piston ring-pack friction. In: *Proceedings of the 2004 fall technical conference of the ASME internal combustion engine division*. Long Beach, California, USA, 2004, pp.841–849.
5. Spencer A, Almqvist A and Larsson R. A numerical model to investigate the effect of honing angle on the hydrodynamic lubrication between a combustion engine piston ring and cylinder liner. *Proc IMechE Part J: J Engineering Tribology* 2011; 257: 683–689.
6. Mezghani S, Demirci I, Mansori ME, et al. Mutual influence of crosshatch angle ad superficial roughness of honed surfaces on friction in ring-pack tribo-system. *Tribol Int* 2013; 66: 540–559.
7. Caciu C, Decenciere E and Jeulin D. Parametric textured surfaces for friction reduction in combustion engine. *Tribol Trans* 2008; 51: 533–541.
8. Tomanik E. Friction and wear bench tests of different engine liner surface finishes. *Tribol Int* 2008; 41: 1032–1038.
9. Pawlus P. A study on the functional properties of honed cylinders surface during running-in. *Wear* 1994; 176: 247–254.
10. Mcgeehan JA. A literature review of the effects of piston and ring friction and lubricating oil viscosity and fuel economy. *SAE Paper* 1978; 780673.
11. Srivastava DK, Agarwal AK and Kumar J. Effect of liner surface properties on wear and friction in a non-firing engine simulator. *Mater Des* 2007; 28: 1632–1340.
12. Sabri L, Mezghani S, El Mansori M, et al. Multiscale study of finish honing process in mass production of cylinder liner. *Wear* 2011; 271: 509–513.
13. Sabri L, Mezghani S and El Mansori M. Functional optimisation of production by honing engine cylinder liner. *Mech Ind* 2010; 11: 365–377.
14. Johansson S, Nilsson PH, Ohlsson R, et al. New cylinder surfaces for low oil consumption. *Tribol Int* 2008; 41: 854–859.
15. Haasis G and Weigmann UP. New honing technique reduces oil consumption. *Diamond Rev* 1999; 59: 205–211.
16. Dimkovski Z, Cabanettes F, Lofgren H, et al. Optimization of cylinder liner surface finish by slide honing manufacture. *Proc IMechE Part B: J Engineering Manufacture* 2010; 226: 575–584.
17. Hoen T, Schmid J and Stumpf W. Less wear and oil consumption trough helical slide honing of engines by deutz. *MTZ Worldwide* 2009; 70: 46–51.
18. Malburg MC and Raja J. Characterization of surface texture generated by plateau honing process. *CIRP Ann* 1993; 42: 637–639.

19. Mainsah E, Greenwood JA and Chetwynd DG. *Metrology and properties of engineering surfaces.* Boston: Kluwer Academic Publishers, 2001, pp.263–276.

20. Demirci I, Mezghani S, Yousfi M, et al. The scale effect of roughness on hydrodynamic contact friction. *Tribol Trans* 2012; 55: 705–712.

21. Larson R. Modelling the effect of surface roughness on lubrication in all regimes. *Tribol Int* 2009; 42: 512–516.

22. Mezghani S, Demirci I, Zahouani H, et al. The effect of groove texture patterns on piston-ring pack friction. *Precis Eng* 2012; 36: 210–217.

23. Yuan S, Huang W and Wang X. Orientation effects of micro-grooves on sliding surfaces. *Tribol Int* 2011; 44: 1047–1054.

24. Krupka I, Perka P, Hartl M, et al. Effect of real longitudinal surface roughness on lubrication film formation with in line elastohydrodynamic contact. *Tribol Int* 2010; 43: 2384–2389.

25. Pawlus P, Cieslak T and Mathia T. The study of cylinder liner plateau honing. *J Mater Process Technol* 2009; 209: 6078–6086.

26. Reizer R and Pawlus P. 3D surface topography of cylinder liner forecasting during plateau honing process. *J Phys Conf Ser* 2011; 311: 012021.

27. Zahouani H, Mezghani S, Vargiolu R, et al. Identification of manufacturing signature by 2d wavelet decomposition. *Wear* 2008; 26: 480–485.

28. Patir N and Cheng HS. An average flow model for determining effects of three-dimensional roughness on partial hydrodynamic lubrication. *J Tribol* 1978; 100: 12–17.

29. Hu YZ and Zhu D. Full numerical solution to the mixed lubrication in point contacts. *J Tribol* 2000; 122: 1–9.

30. Yang P and Wen S. A generalized Reynolds equation for non-Newtonian thermal elastohydrodynamic lubrication. *J Tribol* 1990; 112: 631–636.

31. Elrod EG and Adams M. A computer program for cavitation and starvation problems. In: *First Leeds-Lyon symposium on cavitation and starvation and related phenomena in lubrication*, 1974; 103: 37–41.

32. Ausas RF, Jai M and Buscaglia GC. A mass-conserving algorithm for dynamical lubrication problems with cavitation. *J Tribol* 2009; 131: 1–7.

33. Bair S. A rough shear-thinning correction for EHD film thickness. *Tribol Trans* 2004; 47: 361–365.

34. Habchi W. *A full-system finite element approach to elastohydrodynamic lubrication problems: application to ultra-low-viscosity fluids.* PhD Thesis, INSA de Lyon, France, 2008.

35. Venner CH and Morales-Espejel G. Amplitude reduction of small-amplitude waviness in transient elastohydrodynamically lubricated line contacts. *Proc IMechE Part J: J Engineering Tribology* 1999; 213: 487–504.

36. Venner CH and Lubrecht AA. *Multilevel methods in lubrication.* Amsterdam: Elsevier, 2000.

37. Liu SB, Wang Q and Liu G. A versatile method of discrete convolution and FFT (DC-FFT) for contact analyses. *Wear* 2000; 243: 101–111.

38. Chen WW, Liu SB and Wang Q. Fast Fourier transform based numerical methods for elasto-plastic contacts with nominally flat surface. *J Appl Mech* 2008; 75: 011022.

39. Chapkov A. *Etude des contacts elastohydrodynamique lubrifiees avec un fluide Non-Newtonien.* PhD Thesis, INSA de Lyon, France, 2006.

40. Ren N, Zhu D, Chen WW, et al. Plasto-elastohydrodynamic lubrication (PEHL) in point contacts. *J Tribol* 2010; 132: 031501.

41. Demirci I, Mezghani S, Yousfi M, et al. Multiscale analysis of the roughness effect on lubricated rough contact. *J Tribol* 2014; 136: 011501–1-8.